Probing local structural fluctuations in myoglobin by size-dependent thiol-disulfide exchange

Margaret M. Stratton, Thomas A. Cutler, Jeung-Hoi Ha, and Stewart N. Loh*

Department of Biochemistry and Molecular Biology, State University of New York Upstate Medical University, Syracuse, New York 13210

Received 18 March 2010; Revised 28 April 2010; Accepted 4 June 2010
DOI: 10.1002/pro.440
Published online 23 June 2010 proteinscience.org

Abstract: All proteins undergo local structural fluctuations (LSFs) or breathing motions. These motions are likely to be important for function but are poorly understood. LSFs were initially defined by amide hydrogen exchange (HX) experiments as opening events, which expose a small number of backbone amides to $^{1}H/^{2}H$ exchange, but whose exchange rates are independent of denaturant concentration. Here, we use size-dependent thiol-disulfide exchange (SX) to characterize LSFs in single cysteine-containing variants of myoglobin (Mb). SX complements HX by providing information on motions that disrupt side chain packing interactions. Most importantly, probe reagents of different sizes and chemical properties can be used to characterize the size of structural opening events and the properties of the open state. We use thiosulfonate reagents (126–274 Da) to survey access to Cys residues, which are buried at specific helical packing interfaces in Mb. In each case, the free energy of opening increases linearly with the radius of gyration of the probe reagent. The slope and the intercept are interpreted to yield information on the size of the opening events that expose the buried thiol groups. The slope parameter varies by over 10-fold among Cys positions tested, suggesting that the sizes of breathing motions vary substantially throughout the protein. Our results provide insight to the longstanding question: how rigid or flexible are proteins in their native states?

Keywords: folding; SX; hydrogen exchange; breathing; unfolding; subglobal unfolding; dynamics

Introduction

Studying the dynamic characteristics of native proteins remains a challenge in protein chemistry. Dynamic experiments inform us that the native state is not a rigid entity; rather, it is an amalgam of conformations that fluctuate about a mean structure. These fluctuations range from small breathing motions [local structural fluctuations (LSFs)] to whole molecule unfolding. LSFs provide native proteins with dynamic motion, which can be essential for function. For example, binding generally requires some structural rearrangements to accommodate the ligand.[1–3] In particular, cooperative binding appears to be facilitated by dynamic motion of the polypeptide chain, which often allows distant binding sites to communicate with one another.[4] Finally, local motions have been linked to elementary catalytic steps for a number of enzymes including triosephosphate isomerase,[5–7] ribonuclease A,[8,9] and dihydrofolate reductase.[10,11]

Amide hydrogen exchange (HX) and thiol-disulfide exchange (SX) are uniquely suited to characterize structural fluctuations in proteins. HX refers to exchange of a hydrogen ion from a backbone amide group with one from the solvent. SX is analogous to HX except that the exchanging species are a Cys side chain and a thiol-reactive reagent added to the solvent. Both processes are modeled by the Linderstrøm–Lang mechanism [Eq. (1)]

Additional Supporting Information may be found in the online version of this article.

*Correspondence to: Stewart N. Loh, Department of Biochemistry and Molecular Biology, State University of New York Upstate Medical University, 750 East Adams Street, Syracuse, NY 13210. E-mail: lohs@upstate.edu

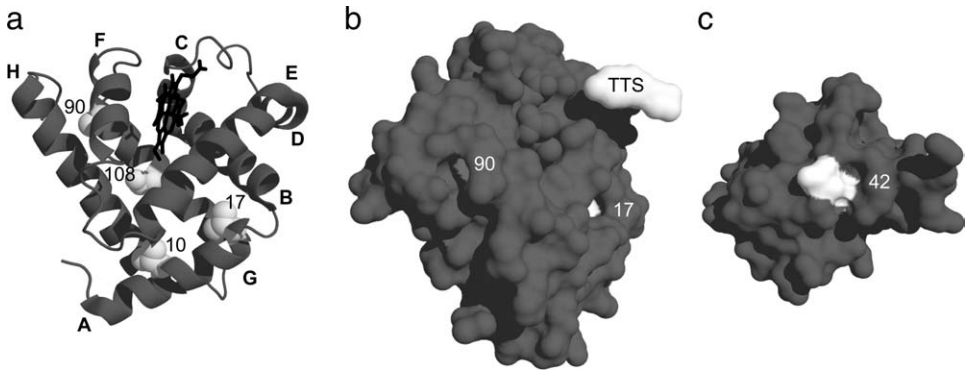

Figure 1. X-ray structures of WT Mb and WT Ub. (a) Ribbon diagram of Mb depicting the side chains of Val10, Val17, Ala90, and Ser108 as white space-filling spheres and the heme group as black sticks. Helices are indicated A–H. (b) Solvent-accessible surface of Mb, presented in the same view as in (a). The side chains of Ala90 and Val17 (white) are slightly exposed; the side chains of Val10 and Ser108 are completely buried and not visible. The TTS probe is drawn to scale. (c) Solvent-accessible surface of Ub with the side chain of Arg42 shown in white.

$$\text{Closed} \overset{K_{op}}{\rightleftarrows} \text{Open} \overset{k_{int}}{\rightarrow} \text{Exchange} \qquad (1)$$

where K_{op} is the equilibrium constant between open and closed states and k_{int} is the intrinsic exchange rate in the absence of structure. The EX2 condition is shown in which open and closed states equilibrate rapidly with respect to k_{int}. In the EX2 limit, the observed exchange rate (k_{obs}) is given by $k_{obs} \cong K_{op} \cdot k_{int}$ and the free energy associated with the opening reaction (ΔG_{op}^{HX} or ΔG_{op}^{SX}) is equal to $-RT \cdot \ln K_{op}$. Exchange takes place according to three classes of structural opening events, in order of increasing size: LSFs, subglobal unfolding, and global unfolding. Subglobal and global unfolding events are identified by an increase in k_{obs} with denaturant concentration. Virtually, all amide and thiol groups exchange by subglobal or global unfolding at sufficiently high-denaturant concentration.[12] By contrast, exchange rates of groups exposed by LSFs are independent of denaturant concentration, signifying that little surface area is uncovered in these fluctuations. LSFs tend to be low-energy, high-probability events. As evidence, most backbone hydrogens exchange via LSFs in the absence of denaturant.[13,14] LSFs are a rich source of dynamic information, which has been largely unexplored.

HX has been the main tool used to characterize LSFs to date. Using 2D NMR, HX rates can be measured for many residues simultaneously and in a nonperturbing fashion.[13,15–17] The limitations of HX/NMR are: (i) probe molecules are restricted to hydrogen ion isotopes, (ii) the data are only indicative of opening reactions that expose the backbone amides to exchange, and (iii) resonance assignments are required. With respect to the last point, mass spectrometry detection negates the need for assignment and extends the protein size limit considerably but comes at the expense of residue-specific resolution.

SX complements HX by addressing the limitations described above. The principle advantage of SX is that one can use an extensive selection of thiol-reactive probe reagents to investigate the size and properties of opening reactions. Moreover, SX reports on events that expose buried side chains (rather than backbone amides) to the solvent. Finally, because SX can be monitored by techniques such as absorbance, fluorescence, and mass spectrometry, the protein size limitation is largely eliminated and site-specific resolution is retained. The disadvantage of SX is that Cys-containing mutants must be created and tested for possible perturbation of structure or stability. To facilitate this process, the Harbury group has developed a method for rapidly generating and analyzing large libraries of single-Cys mutants.[18]

Here, we use thiosulfonate (TS) compounds as probe reagents. TSs react rapidly and specifically with thiolate groups. We selected four compounds ranging in size from the smallest commercially available TS [methyl methanethiosulfonate (MMTS)] to one of the largest ([2-trimethylammonium)ethyl] toluenethiosulfonate, TTS). For the target protein, we use sperm whale myoglobin (Mb) with its heme group in the water-bound ferric state. Wild-type (WT) Mb contains no Cys residues. In a previous study, we created 10 single-Cys mutants and measured their SX rates as a function of urea and guanidine hydrochloride (GdnHCl) concentration using the bulky reagent 5,5′-dithiobis(2-nitrobenzoic acid) (DTNB).[19,20] At low-denaturant concentrations, ΔG_{op}^{SX} values were significantly higher for DTNB than for MMTS at most sites. This disparity suggests that the size difference between reagents can be exploited to estimate the amplitudes of the structural opening events. The purpose of the work presented here is to further investigate the size dependence of SX by using intermediately sized thiol probes to characterize LSFs at helical packing interfaces in Mb.

Results

Mb mutants and thiol probe reagents

We chose to study the V10C, V17C, A90C, and S108C Mb mutants for the following reasons: (i)

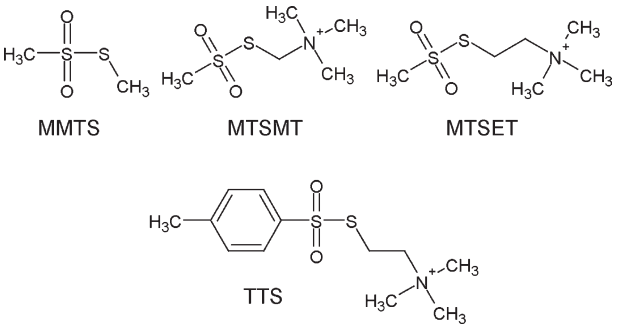

Figure 2. Chemical structures of thiosulfonate probe reagents.

Their side chains are buried at representative helical packing interfaces: A-H (V10C), A-B-G (V17C), F-H (A90C), and G-H (S108C) [Fig. 1(a)].[21] The A-B-G-H helices constitute the stable core of Mb and are known to fold first,[22] whereas the F helix folds last and only in the presence of heme.[23] (ii) Subsitution with Cys at these positions does not destabilize Mb substantially.[20,21,24] (iii) These side chains exhibit slow SX rates, consistent with their high degree of burial in the X-ray structure [Fig. 1(b)], yet they are known to exchange via LSFs.[20] (iv) Our previous study suggested that ΔG_{op}^{SX} is dependent on probe size at each of these positions.

Figure 2 shows the four TS reagents used in this study: MMTS, [1-(trimethylammonium)methyl] methanethiosulfonate (MTSMT), [2-(trimethylammonium)ethyl] methanthiosulfonate (MTSET), and TTS. Ideally, k_{int} values are obtained using unfolded protein as the substrate (as opposed to short peptides). To do so, we denatured heme-free Mb (apoMb) S108C in 2*M* GdnHCl. Because TS reagents exchange rapidly with exposed thiols, it was necessary to slow the reaction by lowering pH to 5.0. The second-order intrinsic rate constants (k_{int}^{2nd}) were measured for each TS in 2*M* GdnHCl, pH 5.0 and corrected to match experimental conditions (0*M* GdnHCl, pH 7.0) by applying the extrapolation terms described in section Materials and Methods. The corrected k_{int}^{2nd} values are listed in Table I. k_{int} (which is a pseudo first-order rate constant) was then calculated for each experiment by multiplying the k_{int}^{2nd} values in Table I by the TS concentration used in that experiment. We previously determined that k_{int} varies by no more than a factor of two among the Cys mutants tested[25]; therefore, the k_{int} values obtained for apoMb S108C were used for all variants. Available data indicate that LSFs are rapid and result in EX2-limited exchange.[13,26,27] As a test, we measured SX rates for Mb A90C using three concentrations of MMTS. Log k_{obs} increased linearly with log·[MMTS] (slope = 0.90, R^2 = 0.98; data not shown), verifying the EX2 condition. Sizes of the TS probes were estimated by calculating their radii of gyration (R_g) using SYBYL 6.5.[28] These values are summarized in Table I.

Figure 3 shows representative data collected in triplicate for the reaction of Mb S108C with MMTS. Mb is reacted with at least a fivefold excess of TS probe to ensure pseudo first-order kinetics. At the indicated time points, the reaction is quenched by free Cys and desalted. Free protein thiol groups are then labeled with Texas Red (TR) methylthiosulfonate (TRMTS) in denaturing solution. Following a second desalting step to remove unreacted TRMTS, the fraction of free thiol is determined by the molar ratio of protein-bound TR to protein (measured by absorbance). As shown in Figure 3, the data fit to a one-exponential function, which decays approximately to zero. This result is expected and is representative of the majority of data collected. In few select reactions, the signal decayed to a level significantly above zero (not shown). This finding indicates that a fraction of protein was extremely slow to react under native conditions, but reacted normally with TRMTS in 6*M* GdnHCl. The most likely source of this unreacted material is a minor population of aggregated protein. In these cases, the rate observed for the major, faster-reacting population is reported. Table II summarizes the calculated ΔG_{op}^{SX} values.

SX at a solvent-exposed site

Our goal is to use probes of different sizes to investigate the nature of open states. To establish a benchmark for comparison, we first examine the exchange behavior of a Cys residue at a surface site (position 42) on a folded protein [ubiquitin (Ub)]. The side chain of Arg42 is fully exposed in the X-ray structure of WT Ub [Fig. 1(c)] and exchange of Cys42 in the R42C mutant is expected to occur without a major structural opening event that would require movement of backbone atoms. However, because Cys42 is surrounded by folded structure, it likely

Table I. *Characteristics of Thiol Probes*

Chemical name	Abbreviation	k_{int}^{2nd} (M^{-1} s^{-1})[a]	R_g (Å)
Methyl methanthiosulfonate	MMTS	2550	1.651
[1-(Trimethylammonium)methyl] methanethiosulfonate	MTSMT	46,180	2.473
[2-(Trimethylammonium)ethyl] methanethiosulfonate	MTSET	30,230	2.905
[2-(Trimethylammonium)ethyl] toluenethiosulfonate	TTS	281,900	3.419

[a] pH 7.0, 0°C.

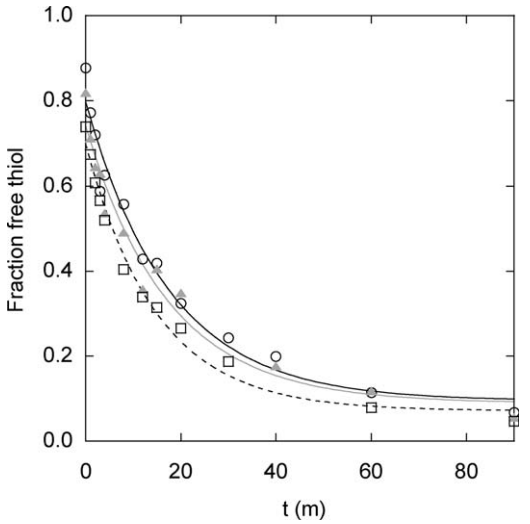

Figure 3. Representative SX data for Mb S108C and MMTS. Data points are from three separate experiments performed on different days (open circles, closed gray triangles, and open squares). The lines are the best fits of each data set to a single exponential function.

mimics the open state of LSFs more realistically than short peptides or denaturant-unfolded proteins.

Figure 4(a) shows the correlation between ΔG_{op}^{SX} and R_g for Ub R42C. One might expect a priori that each probe would exchange at its intrinsic rate. If so, the correlation would follow a flat line with slope (m^{R_g}) and y-intercept (ΔG_{op}^{Rg}) equal to zero. Surprisingly, all of the TS probes exchange significantly more slowly (100- to 3400-fold) than k_{int} and the data are minimally fit by a line with $m^{R_g} > 0$. There are two limiting explanations for why $k_{obs} < k_{int}$.

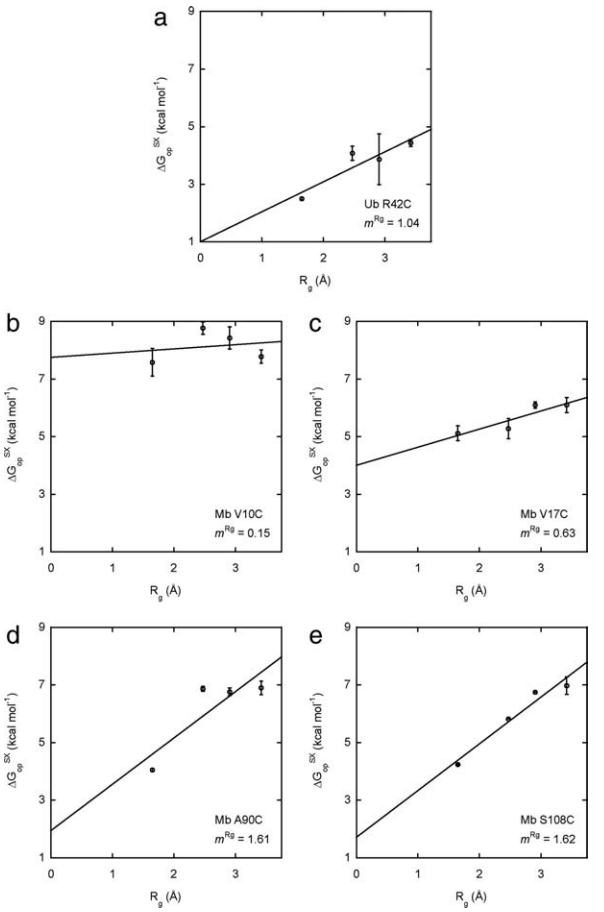

Figure 4. Dependence of ΔG_{op}^{SX} on R_g for Ub and Mb variants. The locations of the Cys reporter residues and the slopes of the fitted lines are indicated in each panel (m^{R_g} values are in units of kcal/mol/Å). Error bars are standard deviations of at least three experiments.

Table II. *SX Parameters for Ub and Mb Variants*

Variant	Probe reagent	ΔG_{op}^{SX} (kcal mol^{-1})	m^{R_g} (kcal/mol/Å)	ΔG^{R_g} (kcal mol^{-1})
Ub R42C	MMTS	2.50 ± 0.048	1.04	1.00
	MTSMT	4.08 ± 0.25		
	MTSET	3.87 ± 0.88		
	TTS	4.44 ± 0.12		
Mb V10C	MMTS	7.58 ± 0.48	0.15	7.76
	MTSMT	8.77 ± 0.21		
	MTSET	8.43 ± 0.39		
	TTS	7.78 ± 0.23		
Mb V17C	MMTS	5.12 ± 0.26	0.63	4.01
	MTSMT	5.28 ± 0.35		
	MTSET	6.10 ± 0.11		
	TTS	6.10 ± 0.26		
Mb A90C	MMTS	4.05 ± 0.052	1.61	1.95
	MTSMT	6.87 ± 0.088		
	MTSET	6.76 ± 0.13		
	TTS	6.90 ± 0.23		
Mb S108C	MMTS	4.24 ± 0.021	1.62	1.95
	MTSMT	5.82 ± 0.004		
	MTSET	6.75 ± 0.005		
	TTS	6.98 ± 0.3		

Errors are standard deviations of at least three measurements.

The first is that Cys42 in native Ub and Cys108 in GdnHCl-denatured apoMb both exchange in an unhindered manner, but the pK_a of Cys42 is higher than that of Cys108. Cys42 would thus exchange more slowly than Cys108 because a greater percentage of the Cys42 thiol exists in protonated form. A difference in pK_a values would presumably arise from either a high concentration of negative charge surrounding Cys42 or a high concentration of positive charge surrounding Cys108. The electrostatic potential around Cys42 in native Ub is known to be positive[29] and the only charged residue close in sequence to Cys108 is Glu109. Most importantly, however, a pK_a difference would simply displace the y-intercept of the ΔG_{op}^{SX} versus R_g correlation by a constant increment. In this case, the slope would not deviate from zero, as we observe in our data.

The second and more likely scenario is that the discrepancy between the Ub R42C and apoMb S108C rates is due to differences in the dynamic properties of the open states. The exchange-competent state of

Cys42 is the surface of a folded protein in which nearby side chains and backbone groups are constrained in space by native structure. The rugged features of the surrounding landscape may hinder access to the Cys side chain. By contrast, the open state of Cys108 is the GdnHCl-denatured form, which lacks persistent structure and is much more flexible. This view also provides an explanation for the positive slope of ΔG_{op}^{SX} versus R_g [Fig. 4(a)]. Figure 4(a) indicates that on the surface of folded Ub, larger probe reagents are hindered to a greater extent than smaller reagents. This phenomenon is less pronounced or altogether absent in GdnHCl-denatured apoMb. Existing SX and HX studies use either GdnHCl-denatured proteins or short peptides to model the open state. Although this may be appropriate when exchange occurs via global unfolding, an open state such as that of R42C Ub may better reflect the locally unfolded conformations from which LSFs and subglobal exchange takes place.

SX at buried locations

Figure 4(b–e) shows SX results for Mb V10C, V17C, A90C, and S108C, respectively. For most variants, the points fit satisfactorily to a straight line, and we analyze the data using the same m^{R_g} and ΔG_{op}^{Rg} parameters as above. This interpretation assumes that the logarithm of the exchange rate depends linearly on R_g values of the probe reagents. However, it is important to recognize that this relationship is purely empirical. To our knowledge, there is no theoretical model from which the dependence of exchange rate on R_g can be derived. We assume linearity because it fits the data using the minimum number of parameters.

Table II summarizes m^{R_g} and ΔG_{op}^{Rg} values obtained from the linear fits of the data in Figure 4. A large ΔG_{op}^{Rg} value implies an unfavorable event, which may involve breaking a number of interactions. A ΔG_{op}^{Rg} value of $\leq$1 kcal/mol is comparable with that observed for a surface-exposed thiol group and indicates a low-energy fluctuation. It is reasonable to intuit that ΔG_{op}^{Rg} is proportional to the physical size of the opening event, although this is not necessarily so. Instead, we propose that the physical size of the fluctuation is reported primarily by m^{R_g}. If the amplitude of the fluctuation is smaller than or comparable with R_g, then smaller probe reagents will react more rapidly than larger molecules. This relationship leads to a positive deflection in the ΔG_{op}^{SX} versus R_g plot, which is manifested by $m^{R_g} > 0$ in the linear model. If the opening size is larger than the largest TS, then ΔG_{op} will be independent of probe size and $m^{R_g} = 0$. m^{R_g} for R42C Ub [1.0 kcal/mol/Å; Fig. 4(a)] establishes a reference for the size-dependence of exchange for a Cys residue, which is solvent-exposed but surrounded by native structure. The m^{R_g} values for V10C (0.15 kcal/mol/Å) and V17C (0.63 kcal/mol/Å) are lower than that of the surface Cys control. This result suggests that at these sites the amplitudes of the LSFs are larger than the R_g of the largest probe (3.4 Å). Large fluctuations are expected to be high-energy, low-probability events. Accordingly, ΔG_{op}^{Rg} values for these mutants are significantly higher than that of the Ub R42C control (Table II). By contrast, A90C and S108C exhibit larger slopes than the exposed Cys control (m^{R_g} = 1.6 kcal/mol/Å in each case). The small ΔG_{op}^{Rg} values (1.9 kcal/mol and 1.7 kcal/mol, respectively) support the notion that fluctuations at these sites are comparable with or smaller than R_g of the probe reagents.

Discussion

Conventional native-state HX and SX experiments yield two parameters: ΔG_{op} and the dependence of ΔG_{op} on denaturant. By using probe reagents of varying size, this study introduces two additional parameters, m^{R_g} and ΔG_{op}^{Rg}, which provide new information on the size of structural opening events. For example, consider Cys17 and Cys90. Both side chains exhibit similar degrees of solvent accessibility (Fig. 1). The smallest probe reagent (MMTS) exchanges with Cys90 (ΔG_{op}^{SX} = 4.0 kcal/mol) more readily than with Cys17 (ΔG_{op}^{SX} = 5.1 kcal/mol). However, the largest TS probe (TTS) exchanges more readily with Cys17 (ΔG_{op}^{SX} = 6.1 kcal/mol) than with Cys90 (ΔG_{op}^{SX} = 6.9 kcal/mol). The reason for the switch is because Cys90 exchanges 125-fold more slowly with TTS than with MMTS, whereas Cys17 is relatively insensitive to probe size. The m^{R_g} value of Cys90 is 2.5-fold greater than that of Cys17. This result suggests that the opening event exposing Cys17 is larger than the opening event exposing Cys90.

Cys90 and Cys108 exhibit large m^{R_g} and small ΔG_{op}^{Rg} values, suggesting that the LSFs exposing those side chains occur frequently and are relatively small. Cys90 is located in helix F and Cys108 is found in helix G (Fig. 1). Both side chains pack against side chains in helix H (Ile142 and Leu135/Arg139, respectively). It is possible that minor fluctuations involving a portion of helix H may facilitate exchange at both positions. The side chain of Ser108 is fully buried in the X-ray structure of WT Mb and the side chain of Ala90 is partially accessible (Fig. 1) yet their ΔG_{op}^{Rg} and m^{R_g} values are approximately equal. Small-amplitude LSFs can therefore promote exchange at both partially exposed and well-packed positions.

The small m^{R_g} and large ΔG_{op}^{Rg} values of Cys10 and Cys17 signify that LSFs at these positions are large and relatively rare. Cys10 and Cys17 are both located in helix A. The Val10 side chain is fully buried and it contacts Ala130 and Met131 at the N-terminus of helix H. The A-H interface thus appears to be quite rigid; if small-amplitude LSFs of helix H facilitate exchange at positions 90 and 108, such

fluctuations must be limited to the C-terminal portion of the helix. The side chain of Val17 makes contact with Asp20 and Val21 (helix A), His24 (helix B), and Leu115 (helix G). The packing interfaces between helix A and its neighboring helices thus appear to be quite stable. As noted above, highly buried positions can be exposed by small, low-energy LSFs and the converse is true as well. Cys17 is partially solvent-exposed, yet it requires a large, high-energy LSF to exchange.

It is instructive to compare this work with previous HX and SX studies of Mb. The exchanging species in HX experiments (the hydroxide ion) is smaller than MMTS. Cavagnero *et al.*[30] measured HX rates for CO-bound Mb and these rates were converted to ΔG_{op}^{HX} values according to Eq. (1).[26] Val10, Val17, Ala90, and Ser108 can be categorized into two groups based on these HX data. ΔG_{op}^{HX} values are small for Ala90 and Ser108 (4.3 kcal/mol and 4.6 kcal/mol, respectively) and $\Delta G_{op}^{HX} < \Delta G_{op}^{SX}$ in each case ($\Delta G_{op}^{SX} = 5.0$ kcal/mol for Cys90; $\Delta G_{op}^{SX} = 5.6$ kcal/mol for Cys108), when SX was measured using the bulky DTNB probe.[26] This result is consistent with the large m^{R_g} values measured here for Cys90 and Cys108. In contrast, HX of Val10 and Val17 is associated with large ΔG_{op}^{HX} values (8.2 kcal/mol and 7.7 kcal/mol, respectively) and $\Delta G_{op}^{HX} > \Delta G_{op}^{SX}$ for both residues ($\Delta G_{op}^{SX} = 7.4$ kcal/mol for Cys10; $\Delta G_{op}^{SX} = 6.5$ kcal/mol for Cys17). This finding is in agreement with the notion that positions 10 and 17 are exposed by large-scale, high-energy fluctuations. However, it must be noted that HX and SX data were collected at different pH values, temperatures, and heme ligation states. Therefore, comparisons can be made only on a qualitative basis.

The above discussion considers that each Cys reporter is exposed by an independent fluctuation (with the possible exception of Cys90 and Cys108, which exhibit similar m^{R_g} and ΔG_{op}^{Rg} values). In addition, all probe reagents are envisioned to exchange by the same unique fluctuation at any given site. It is also plausible that, at some sites, more than one fluctuation is involved and the probe reagents differentiate between them based on their size. For example, Cys90 appears to exhibit a bimodal distribution of ΔG_{op}^{SX} values [Fig. 4(d)]. This pattern can be explained by two locally unfolded conformations with ΔG_{op}^{SX} values of ~4 kcal/mol and ~7 kcal/mol, respectively. The lower energy conformation admits MMTS but not MTSMT, MTSET, or TTS. The higher energy fluctuation admits all probe reagents with approximately equal ease. In this scenario, Cys10 would be accessible only in the higher energy conformation. By observing trends such as these using additional Cys reporters and probe reagents, it may be possible to determine whether LSFs at different sites are independent or are linked by a more limited set of opening events.

Our results address a longstanding paradox posed by HX experiments. LSFs are widely regarded as minor breathing motions which expose little solvent-accessible surface and appear to allow only a single amide NH to exchange at a time.[14] Yet LSFs can exhibit ΔG_{op} values that approach ΔG of global unfolding. How can such subtle fluctuations be associated with large opening free energies? Figure 4(a) suggests that part of the answer may be that different k_{int} values apply for global versus subglobal or local unfolding events. HX studies use a common set of reference k_{int} values, which were measured using unstructured model peptides.[31] Short peptides represent the globally unfolded state well, as evidenced by the close agreement between ΔG_{op} and ΔG_{fold} for hydrogens that exchange by whole-molecule unfolding. When exchange occurs from LSFs or sub-global unfolding events, however, only a portion of the molecule opens. One can envision that probe molecules may only be able to approach the amide or thiol group by a limited number of trajectories, as opposed to having full 360° access to sites in the globally denatured protein.[32] Thus, exchange-competent states in LSFs are likely to resemble the solvent-exposed surface of a structured protein moreso than the globally unfolded state. If so, then k_{int} values may be overestimated for hydrogens that exchange by LSF and subglobal mechanisms. This potential problem, which would result in overestimation of ΔG_{op} for LSFs [by as much as 4.4 kcal/mol in this study; Fig. 4(a)], has been discussed by others in the context of HX.[33,34]

In conclusion, we have demonstrated that conformational openings in proteins can be characterized by two new parameters, ΔG^{R_g} and m^{R_g}, which are obtained by size-dependent SX. A freely exchanging Cys on the surface of a folded protein exchanges 100- to 3400-fold more slowly than the intrinsic rates measured with GdnHCl-unfolded protein. Moreover, the former demonstrates an unexpected dependence on probe size that is not exhibited by the latter. Examining four buried positions in Mb reveals that two are exposed to the solvent by small-amplitude fluctuations and two are exposed by larger opening events. The apparent size of the fluctuations is not correlated with extent of side-chain burial, but instead may be dictated by local motions of the helices in Mb.

Materials and Methods

Gene construction and protein purification

The Ub R42C mutation was introduced into the WT Ub gene using the QuikChange kit (Stratagene). Ub and Mb were purified as described.[25,35]

Intrinsic rate measurements

All TS reagents were purchased at the highest purity available from Toronto Research Chemicals.

ApoMb S108C was reduced with tris(2-carboxyethyl)phosphine (TCEP) for 30 min at room temperature then desalted using a PD-10 column (GE Healthcare) into 2*M* GdnHCl, 20 m*M* acetate (pH 5.0). The midpoint of denaturation of apoMb S108C is less than 1*M* GdnHCl (data not shown). ApoMb was mixed with a fivefold excess of each TS to ensure pseudo first-order conditions. SX was quenched at designated time points by excess cysteine. The protein was then precipitated with 10% trichloroacetic acid and unreacted thiol was measured by DTNB assay. The decay of free thiol was fit to a single-exponential function to obtain the pseudo first-order rate constant for each probe reagent (Supporting Information Fig. S1). k_{int}^{2nd} was calculated by dividing the aforementioned rate by the TS concentration. k_{int}^{2nd} values reported in Table I are the average of duplicate measurements.

The dependence of thiol reactivity on pH was determined by measuring the exchange rate of MMTS over the pH range 4.5–5.5. The same GdnHCl-unfolded sample of apoMb S108C was used. ApoMb S108C (15 μ*M*) was mixed with MMTS (100 μ*M*) in 2*M* GdnHCl at pH 4.5, pH 4.75, pH 5.0, and pH 5.5 (0°C). The reaction was quenched and unreacted thiol was measured as above. Plotting log k_{obs} (s^{-1}) versus pH yielded a straight line with a slope of 1.2 (Supporting Information Fig. S2).

The dependence of thiol reactivity on GdnHCl concentration was determined by measuring the rate of DTNB exchange with GdnHCl-unfolded calbindin D_{9k} (I73C variant).[36] In each reaction, calbindin (16 μ*M*) was reacted with DTNB (150 μ*M*) in 50 m*M* Tris (pH 7.5), 20°C. The rate was measured in GdnHCl (4–7*M* concentration) using a Bio-Logic SFM4-Q/S operating in stopped-flow mode (absorbance detection). Plotting k_{obs} against the concentration of GdnHCl yielded a straight line with a slope of $-0.218\ s^{-1}\ M^{-1}$ and a *y*-intercept of 2.02 s^{-1} (Supporting Information Fig. S3).

Thiol-disulfide exchange experiments

Native Mb was reacted with the thiol probes in the absence of denaturant (pH 7.0, 0°C). Lyophilized Mb was resuspended in reaction buffer (100 m*M* sodium phosphate, pH 7.0) to a final concentration of 30–40 μ*M*. Concentrations of TS stock solutions were determined at the beginning of each experiment by titration with TNB ($\varepsilon_{412} = 14{,}100 M^{-1}\ cm^{-1}$). The TS concentration in each experiment was adjusted to bring the exchange reaction into roughly the same time course. The final TS concentration exceeded the Mb concentration by at least fivefold in all cases. After mixing TS and Mb, aliquots were removed at various time points, quenched with excess Cys, and immediately precipitated with 10% trichloroacetic acid. Pellets were washed with ice-cold ddH_2O and stored at −80°C. To quantitate unreacted thiol, protein pellets were thawed, resuspended in 6*M* GdnHCl (pH 5.5) and allowed to react fully with excess TRMTS. A Sephadex G25 spin column was used to remove unreacted TRMTS as well as exchange the buffer to 10 m*M* HCl. TR concentration was determined by absorbance (595 nm) and normalized to Mb concentration, which was determined by measuring sample absorbance at 280 nm and subtracting the calculated TR absorbance at that wavelength. k_{obs} values were obtained by fitting the data to a single exponential decay. K_{op} values were calculated by dividing k_{obs} by k_{int}, where k_{int} was extrapolated to experimental conditions of temperature, pH, and TS concentration using the data in Supporting Information Figures S2 and S3.

To test for EX2 conditions, SX experiments were repeated as above for Mb A90C at MMTS concentrations of 1.0 m*M*, 1.5 m*M*, and 2.0 m*M*. The observed reaction rate increased with the concentration of probe reagent, as expected for the EX2 mechanism.

Acknowledgment

The authors thank Tom Duncan for assistance with R_g calculations and Whitney Oswald for technical assistance.

References

1. Bjorkman AJ, Mowbray SL (1998) Multiple open forms of ribose-binding protein trace the path of its conformational change. J Mol Biol 279:651–664.
2. Luque I, Freire E (2000) Structural stability of binding sites: consequences for binding affinity and allosteric effects. Proteins 4:63–71.
3. Dunn B (2002) Structure and mechanism of the pepsin-like family of aspartic peptidases. Chem Rev 203: 4431–4458.
4. Johnson E, Chazin WJ, Rance M (2006) Effects of calcium binding on the side-chain methyl dynamics of Calbindin D_{9k}: a ^2H NMR relaxation study. J Mol Biol 357:1237–1252.
5. Massi F, Wang C, Palmer AG, III (2006) Solution NMR and computer simulation studies of active site loop motion in triosephosphate isomerase. Biochemistry 45: 10787–10794.
6. Berlow RB, Igumenova TI, Loria JP (2007) Value of a hydrogen bond in triosephosphate isomerase loop motion. Biochemistry 46:6001–6010.
7. Wang Y, Berlow RB, Loria JP (2009) Role of loop-loop interactions in coordinating motions and enzymatic function in triosephosphate isomerase. Biochemistry 48:4548–4556.
8. Loria JP, Berlow RB, Watt ED (2008) Characterization of enzyme motions by solution NMR relaxation dispersion. Acc Chem Res 41:214–221.
9. Watt ED, Shimada H, Kovrigin EL, Loria JP (2007) The mechanism of rate-limiting motions in enzyme function. Proc Natl Acad Sci USA 104:11981–11986.
10. Boehr DD, Dyson HJ, Wright PE (2008) Conformational relaxation following hydride transfer plays a limiting role in dihydrofolate reductase catalysis. Biochemistry 47:9227–9233.
11. Borgia A, Bonivento D, Travaglini-Allocatelli C, Di Matteo A, Brunori M (2006) Unveiling a hidden folding

intermediate in c-type cytochromes by protein engineering. J Biol Chem 281:9331–9336.
12. Englander SW, Mayne L, Krishna MMG (2007) Protein folding and misfolding: mechanism and principles. Q Rev Biophys 40:287–326.
13. Bai Y, Sosnick TR, Mayne L, Englander SW (1995) Protein folding intermediates: native-state hydrogen exchange. Science 269:192–197.
14. Maity H, Lim WK, Rumbley JN, Englander SW (2003) Protein hydrogen exchange mechanism: local fluctuations. Protein Sci 12:153–160.
15. Bai Y, Englander SW (1996) Future directions in folding: the multi-state nature of protein structure. Proteins 24:145–151.
16. Bai Y, Sosnik TR, Mayne L, Englander SW (1995) Protein folding intermediates: native state hydrogen exchange. Science 269:192–197.
17. Jeng M-F, Englander SW (1991) Stable submolecular folding units in a non-compact form of cytochrome c. J Mol Biol 221:1045–1061.
18. Silverman J, Harbury P (2002) Rapid mapping of protein structure, interactions, and ligand binding by misincorporation proton-alkyl exchange. J Biol Chem 277: 30968–30975.
19. Feng Z, Butler MC, Alam SL, Loh SN (2001) On the nature of conformational openings: native and unfolded-state hydrogen and thiol-disulfide exchange studies of ferric aquomyoglobin. J Mol Biol 314:153–166.
20. Ha J-H, Loh SN (1998) Changes in side-chain packing during apomyoglobin folding characterized by a pulsed thiol-disulfide exchange. Nat Struct Biol 5:730–737.
21. Feng Z, Ha J, Loh SN (1999) Identifying the site of initial tertiary structure disruption during apomyoglobin unfolding. Biochemistry 38:14433–14439.
22. Hughson F, Wright P, Baldwin B (1990) Structural characterization of a partly folded apomyoglobin intermediate. Science 249:1544–1548.
23. Jennings PA, Wright PE (1993) Formation of a molten globule intermediate early in the kinetic folding pathway of apomyoglobin. Science 262:892–895.
24. Feng Z, Ha J-H, Loh SN (1999) Identifying the site of inital tertiary structure disruption during apomyoglobin unfolding. Biochemistry 38:14433–14439.
25. Ha J-H, Loh SN (1998) Changes in side chain packing during apomyoglobin folding characterized by pulsed thiol-disulfide exchange. Nat Struct Biol 5:730–737.
26. Feng Z, Butler MC, Alam SL, Loh SN (2001) On the nature of conformational openings: native and unfolded-state hydrogen and thiol-disulfide exchange studies of ferric aquomyoglobin. J Mol Biol 314:153–166.
27. Qian H (1997) Thermodynamic heirarchy and local energetics of folded proteins. J Mol Biol 267:198–206.
28. Grosberg AY, Khocklov AR (1994) Statistical physics of macromolecules. AIP Press: Woodbury.
29. Loladze VV, Ibarra-Molero B, Sanchez-Ruiz JM, Makhatadze GI (1999) Engineering a thermostable protein via optimization of charge-charge interactions on a protein surface. Biochemistry 38:16419–16423.
30. Cavagnero S, Thériault Y, Narula SS, Dyson HJ, Wright PE (2000) Amide proton hydrogen exchange rates for sperm whale myoglobin obtained from ^{15}N-^{1}H NMR spectra. Protein Sci 9:186–193.
31. Bai Y, Milne JS, Mayne L, Englander SW (1993) Primary structure effects on peptide group hydrogen exchange. Proteins 17:87–92.
32. Alberty RA, Hammes GG (1958) Application of the theory of diffusion-controlled reactions to enzyme kinetics. J Phys Chem 62:154–159.
33. Anderson JS, Hernandez G, Lemaster DM (2008) A billion-fold range in acidity for the solvent-exposed amides of *Pyrococcus furiosus* rubredoxin. Biochemistry 47:6178–6188.
34. Anderson JS, Hernandez G, LeMaster DM (2009) Backbone conformational dependence of peptide acidity. Biophys Chem 141:124–130.
35. Cutler T, Loh SN (2007) Thermodynamic analysis of an antagonistic folding-unfolding equilibrium between two protein domains. J Mol Biol 371:308–316.
36. Stratton MM, Mitrea DM, Loh SN (2008) A Ca^{2+}-sensing molecular switch based on alternate frame protein folding. ACS Chem Biol 3:723–732.